AZD4547: An Orally Bioavailable, Potent, and Selective Inhibitor of the Fibroblast Growth Factor Receptor Tyrosine Kinase Family

Paul R. Gavine[2], Lorraine Mooney[1], Elaine Kilgour[1], Andrew P. Thomas[1], Katherine Al-Kadhimi[1], Sarah Beck[1], Claire Rooney[1], Tanya Coleman[1], Dawn Baker[1], Martine J. Mellor[1], A. Nigel Brooks[1], and Teresa Klinowska[1]

Abstract

The fibroblast growth factor (FGF) signaling axis is increasingly implicated in tumorigenesis and chemoresistance. Several small-molecule FGF receptor (FGFR) kinase inhibitors are currently in clinical development; however, the predominant activity of the most advanced of these agents is against the kinase insert domain receptor (KDR), which compromises the FGFR selectivity. Here, we report the pharmacologic profile of AZD4547, a novel and selective inhibitor of the FGFR1, 2, and 3 tyrosine kinases. AZD4547 inhibited recombinant FGFR kinase activity *in vitro* and suppressed FGFR signaling and growth in tumor cell lines with deregulated FGFR expression. In a representative FGFR-driven human tumor xenograft model, oral administration of AZD4547 was well tolerated and resulted in potent dose-dependent antitumor activity, consistent with plasma exposure and pharmacodynamic modulation of tumor FGFR. Importantly, at efficacious doses, no evidence of anti-KDR–related effects were observed, confirming the *in vivo* FGFR selectivity of AZD4547. Taken together, our findings show that AZD4547 is a novel selective small-molecule inhibitor of FGFR with potent antitumor activity against FGFR-deregulated tumors in preclinical models. AZD4547 is under clinical investigation for the treatment of FGFR-dependent tumors. *Cancer Res; 72(8); 2045–56. ©2012 AACR.*

Introduction

Fibroblast growth factors (FGF) and their receptors carry out key roles in multiple biologic processes including tissue repair, hematopoiesis, angiogenesis, and embryonic development. The FGF receptor (FGFR) family comprises 4 main members (FGFR1–4), some of which have multiple protein isoforms as a consequence of alternative splicing (1). FGFRs have a core structure containing an extracellular ligand-binding domain, a hydrophobic transmembrane domain, and an intracellular kinase domain. FGF ligand binding results in FGFR dimerization, followed by receptor autophosphorylation and activation of downstream signaling pathways. In addition to the vast complexity of a system represented by 4 receptors and 18 ligands, additional control is provided by the interaction of heparin and heparin sulphate proteoglycans, which modulate ligand binding to receptor (2). Cell- and tissue-specific receptor expression patterns provide a final level of control, which reflects their differential roles across a variety of tissues and cell lineages.

Aside from their normal physiologic roles described above, FGFs and FGFRs are emerging as oncogenes that drive proliferation of a significant proportion of human tumors and that can also mediate resistance to both cytotoxic and targeted agents. Deregulation of FGFR signaling has been documented in clinical samples of breast (3), multiple myeloma (4), bladder (5), endometrial (6), gastric (7), and prostate cancers (8). The most frequently reported tumor-associated finding is receptor overexpression due to gene amplification or aberrant transcriptional regulation. Consequently, tumor cells acquire enhanced sensitivity to FGF ligands or become activated through spontaneous ligand-independent dimerization (9–13). Genetically altered forms of FGFR proteins (e.g., chimeric, truncated, and mutated) have also been identified in human tumors, resulting in receptors, which are either constitutively active or exhibit altered ligand dependence (12, 14). Moreover, receptor activation through gene fusion is exemplified by the discovery of numerous FGFR1 fusion proteins in myeloproliferative disorders (15–17). Finally, FGF2 and FGFR4 have both been associated with protection against etoposide- and doxorubicin-induced apoptosis *in vitro* (18–21), whereas increased

Authors' Affiliations: [1]AstraZeneca R&D, Alderley Park, United Kingdom; and [2]Innovation Center China, AstraZeneca R&D, Shanghai, China

Note: Supplementary data for this article are available at Cancer Research Online (http://cancerres.aacrjournals.org/).

S. Beck was formerly affiliated to AstraZeneca.

Presented in part at AACR 2011 by P.R. Gavine (poster number 3568—Characterization of AZD4547: An orally bioavailable, potent, and selective inhibitor of FGFR tyrosine kinases 1, 2, and 3) and A.N. Brooks (oral presentation in "drug development: special session (new drugs on the horizon 1)" — title: Preclinical profile of AZD4547: A selective inhibitor of FGF receptors 1, 2, and 3).

Corresponding Author: Paul R. Gavine, AstraZeneca Innovation Center China, Building 7, 898 Halei Road, Zhangjiang Hi-Tech Park, Shanghai 201203, PR China. Phone: 0086-15-801994860; Fax: 0086-21-61097700; E-mail: paul.gavine@astrazeneca.com

doi: 10.1158/0008-5472.CAN-11-3034

circulating FGF2 levels show an association with tumor progression following clinical suppression of VEGF signaling (22, 23).

Blockade of FGF/FGFR signaling as a therapeutic approach to cancer is gaining momentum with a number of targeted kinase inhibitors currently in development. The most clinically advanced of these agents are mainly mixed kinase inhibitors with dominant anti-KDR (kinase insert domain receptor) pharmacology (brivanib alaninate; ref. 24), dovitinib (11), BIBF-1120 (25), and SU6668 (26). As such, their anti-FGFR activity is often relatively weak and thus, we do not believe that these agents offer the opportunity to fully test the anti-FGFR hypothesis because of the confounding effects of their other pharmacologic mechanisms. Accordingly, we postulate that there is a need for compounds that are more FGFR-selective, which can be used to more robustly test the FGFR tumor–driven hypothesis. In this report, we describe the preclinical profile of AZD4547, a potent and selective FGFR tyrosine kinase inhibitor currently in phase I clinical studies.

Materials and Methods

AZD4547

N-[5-[2-(3,5-Dimethoxyphenyl)ethyl]-2*H*-pyrazol-3-yl]-4-(3,5-diemthylpiperazin-1-yl)benzamide (AZD4547, AstraZeneca; Fig. 1) was synthesized according to the processes described in the International Patent Application Publication Number WO2008/075068, in particular as described in Example 80. The free base of AZD4547 (molecular weight = 463.6) was used in all preclinical studies. For *in vitro* studies, AZD4547 was prepared as a 10 mmol/L stock solution and diluted in the relevant assay media. For *in vivo* studies, AZD4547 was formulated in a 1% (v/v) solution of polyoxyethylenesorbitan monooleate (Tween-80) in deionized water. Animals were given AZD4547 (1.5–50 mg/kg) or vehicle control once daily or twice daily by oral gavage.

Cell culture

KG1a, Sum52-PE, MCF7, and KMS11 cell lines were routinely grown in RPMI-1640 supplemented with 10% (v/v) fetal calf serum (FCS; Biochrom AG) and 2 mmol/L L-glutamine (Invitrogen). The KMS11 cell line was obtained from Jonathan Keats (Scottsdale, Arizona), KG1a from American Type Culture Collection, MCF7 from the Imperial Cancer Research Fund, and Sum52-PE from Asterand. These cell lines were genetically tested and authenticated with the Powerplex 16 System (Promega) and were not cultured for more than 6 months before conducting the work described here.

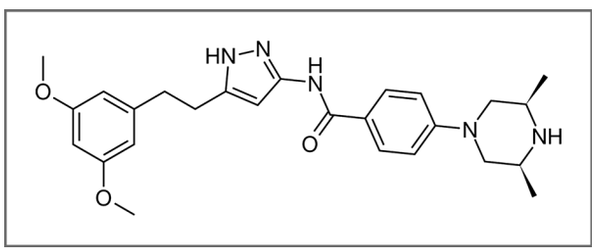

Figure 1. Chemical structure of AZD4547.

Inhibition of cellular receptor phosphorylation

For FGFR phosphorylation studies, FGFR1, 3, or 4–transfected Cos-1 cells were cultured in Dulbecco's Modified Eagle's Medium (DMEM) supplemented with 2 mmol/L L-glutamine and 3% FCS. For FGFR2, Sum52-PE cells were cultured in RPMI-1640 (Gibco), growth media supplemented with 2 mmol/L L-glutamine and 10% FBS. Following 1-hour incubation with AZD4547, media were removed; cells were fixed, permeabilized, and then incubated with monoclonal anti-phospho-FGFR antibody (Cell Signaling Technology; 1:1,000) for 1 hour followed by incubation with anti-mouse Alexa Fluor 594 secondary antibody (1:500) and Hoechst (1:1,000) for 1 hour. Fluorescence measurement was conducted with Arrayscan (Cellomics).

For KDR phosphorylation studies, primary human umbilical vein endothelial cells were obtained from PromoCell and cultured according to the supplier's protocol. Cells were incubated with AZD4547 for 90 minutes and then stimulated for 5 minutes with VEGF ligand (25 ng per well). Cells were lysed with standard radioimmunoprecipitation assay buffer containing phosphatase/protease inhibitors. Lysates were analyzed with the human phospho-VEGF R2 (KDR; R&D systems) ELISA protocol according to the manufacturer's instructions.

For insulin-like growth factor-1 receptor (IGF1R) phosphorylation studies, R^+ cells were derived from murine transgenic IGF1R knockouts and then stably transfected with human IGF1R. Cells cultured in DMEM (Gibco) supplemented with 1% heat-inactivated FCS and 1% L-glutamine were incubated with AZD4547 and then stimulated with IGF ligand (Gropep IMOOl), followed by fixation, blocking, and incubation with a rabbit anti-phospho IGF1R/IR antibody (Biosource;1:350) for 1 hour. Secondary detection and measurement was carried out with an Acumen Explorer HTS Reader (TTP Labtech Ltd.) at an excitation wavelength of 488 nm and emission wavelength of 530 nm.

In vitro protein expression analysis and kinase inhibition studies

Cells were treated with AZD4547 or control for 3 hours at 37°C and then stimulated with 10 ng/mL aFGF/bFGF (Sigma) and 10 μg/mL heparin for 20 minutes. Western blotting was conducted with standard SDS-PAGE procedures and antibody incubation carried out overnight at 4°C. Antibodies were obtained from the following sources: FGFR1 (Epitomics), FGFR2 and FRS2 (R&D Systems), FGFR3 proteins (Abcam), α-tubulin-B512 and Bcl2 (C2; Santa Cruz), and BIM (Millipore). All other antibodies were sourced from Cell Signalling Technologies. Secondary antibodies were applied and immunoreactive proteins visualized with "SuperSignal West Dura" Chemiluminescence substrate according to the manufacturer's instructions (Pierce).

In vitro cell line proliferation studies

In vitro antiproliferative activity was measured as described previously (27). Each experiment was carried out at least in triplicate and data presented as geometric means.

In vitro cell-cycle and apoptotic induction analysis

Cell lines were incubated with fixed concentrations of AZD4547 for 72 hours. For fluorescence-activated cell sorting (FACS), cells were fixed with 70% ethanol and then incubated with propidium iodide/RNase A (Sigma) labeling solution. Cell-cycle profiles were assessed with a FACSCalibur instrument and CellQuest analysis software (Becton Dickinson). For apoptotic analysis, cells and media were gently harvested and centrifuged, followed by washing of cell pellets. Cells were then processed for Annexin V-fluorescein isothiocyanate (FITC) staining and propidium iodide uptake according to the manufacturer's instructions (Abcam). The proportion of cells staining positive for Annexin V were then assessed with a FACSCalibur instrument and quadrant sorting was done by CellQuest analysis software (Becton Dickinson).

Murine plasma pharmacokinetic analyses

Plasma samples were extracted by protein precipitation in acetonitrile, followed by liquid chromatography/tandem mass spectrometry (LC/MS-MS) detection. In short, plasma samples and standards were quenched with acetonitrile and internal standard and centrifuged. Supernatant was diluted 10-fold with deionized water and the samples were analyzed by LC/MS-MS with Masslynx and data processed by Quanlynx software (Waters).

Immunohistochemistry

Antigen retrieval was carried out on formalin-fixed, paraffin-embedded tissues with a RHS-1 microwave vacuum processor (Milestone) at 110°C for 5 minutes in (pH 6) retrieval buffer (S1699; Dako) and the following primary antibodies used: custom rabbit polyclonal antibody raised to COOH-terminal peptide of mouse CD31 (CHG-CD31-PI, AstraZeneca; 1:600), mouse monoclonal anti Ki-67 MIB-1 (Dako M7240; 1:100), and rabbit polyclonal anti-cleaved caspase-3 (Asp 175; #9661, Cell Signaling Technology; 1:100). The appropriate Envision or biotinylated rabbit anti-goat immunoglobulin secondary antibodies were used (K4007/K4003; Dako, PK-6101; Vector Laboratories, Inc.) and staining was detected with diaminobenzidine (K3468; Dako). Finally, sections were counterstained with Carazzi's hematoxylin and image analysis was conducted with the Aperio Digital Pathology System (Aperio Technologies, Inc). Analysis thresholds were set and applied to all tumors within the study by the Aperio Micro Vessel Density (MVD) and nuclear software algorithms (CD31, cleaved caspase-3, and Ki-67). MVD was expressed as mean number of CD31-positive vascular structures per mm^2 of viable tumor. Nuclear staining was expressed as a percentage positive score (number of positive nuclei of the total number of nuclei stained).

In vivo tumor studies

Swiss derived nude (*nu*/*nu*) and severe combined immunodeficient mice (SCID; Charles River) were housed in negative-pressure isolators (PFI Systems Ltd.) at AstraZeneca. All experiments were carried out on 8- to 12-week-old female mice in full accordance with the UK Home Office Animal (Scientific Procedures) Act 1986. Tumor xenografts were established by s.c. injection into the left flank with 0.1 mL tumor cells (1×10^6 for LoVo, 1×10^7 for HCT-15, and 1×10^7 for Calu-6) or 0.2 mL (2×10^7 for KMS11 and KG1a) mixed 1:1 with Matrigel (Becton Dickinson), with the exception of LoVo and HCT-15, which did not include Matrigel. Mice were randomized into control and treatment groups when tumors reached the determined size of more than 0.2 cm^3. Tumor volume (measured by caliper), animal body weight, and tumor condition were recorded twice weekly for the duration of the study. Tumor volume was calculated as described previously (28).

Pharmacodynamic studies

Tumor samples and blood were collected from KMS11 tumor–bearing mice at various time points after single dose of either AZD4547 or vehicle. Frozen tumor samples were lysed in 1× cell lysis buffer (Cell Signaling Technologies) containing phosphatase and protease inhibitors (Sigma) with a Fast Prep Homogenizer (MP Biomedicals). Tumor phospho-FGFR3 was measured by ELISA according to the manufacturer's instructions (DYC2719, R&D systems).

In vivo cardiovascular studies

Blood pressure, heart rate, and activity patterns were collected from conscious, unrestrained rats with the commercially available Data Sciences International telemetry system by the methodology described previously (29).

Results

AZD4547 is a highly potent inhibitor of FGFR tyrosine kinases 1 to 3 and shows selectivity versus a range of additional kinases

AZD4547 potently inhibits the tyrosine kinase activities of recombinant FGFR1, 2, and 3 *in vitro* (IC_{50} values of 0.2, 2.5, and 1.8 nmol/L, respectively; Table 1) and displays weaker activity against FGFR4 ($IC_{50} = 165$ nmol/L). *In vitro* drug selectivity was examined against a diverse panel of representative human kinases and AZD4547 shown to inhibit recombinant VEGFR2 (KDR) kinase activity with an IC_{50} of 24 nmol/L. However, when compared with FGFR1, this represents a selectivity of approximately 120-fold. Excellent selectivity for FGFR was observed across a range of unrelated tyrosine and serine/threonine kinases including IGFR (>2,900-fold), CDK2 (>50,000-fold), and p38 (>50,000-fold). Broader kinase selectivity was explored with 0.1 μmol/L of AZD4547 against a range of recombinant kinases incubated with ATP at or near the appropriate enzyme K_m concentration. No enzyme inhibition was detected against ALK, CHK1, EGFR, MAPK1, MEK1, p70S6K, PDGFR, PKB, Src, Tie2, and PI3-kinase (data not shown).

Because of potent AZD4547 recombinant enzyme inhibition, FGFR1–4, IGFR, and KDR were established as cellular phosphorylation assays and used to generate AZD4547 IC_{50} values (Table 1). In cells, AZD4547 potently inhibits autophosphorylation of FGFR1, 2, and 3 tyrosine kinases (IC_{50} values of 12, 2, and 40 nmol/L, respectively; Table 1) and displays weaker inhibition of FGFR4 cellular kinase activity ($IC_{50} = 142$ nmol/L). Significantly weaker inhibitory activity was observed versus cellular KDR and IGFR ligand–induced phosphorylation (IC_{50} values of 258 and 828 nmol/L, respectively), representing approximately 20- and 70-fold selectivity over cellular FGFR1.

Table 1. AZD4547 kinase activity

Kinase	Enzyme IC_{50},[a] nmol/L	Cellular IC_{50}, nmol/L
FGFR1	0.2 ± 0.06	12 ± 3
FGFR3	1.8 ± 0.33	40 ± 1
FGFR2	2.5 ± 0.23	2 ± 0.2
KDR	24 ± 0.001	258 ± 17
FGFR4	165 ± 30.3	142 ± 29
IGFR	581 ± 0.02	828 ± 41
AXL	>2,000	
CDK2	>10,000	
FAK	>10,000	
ROCK2	>50,000	
AKT1	>100,000	
ALK1	>100,000	
p38	>100,000	
PI3Ka	>100,000	

[a]The ability of AZD4547 to inhibit a range of human recombinant kinase activities was tested using ATP concentrations at, or just below, the respective K_m. Data represent the mean ± SEM of at least 3 separate determinations. IC_{50} values denoted as "greater than" denote the inability to reach 50% inhibition of maximal activity at the highest tested concentration.

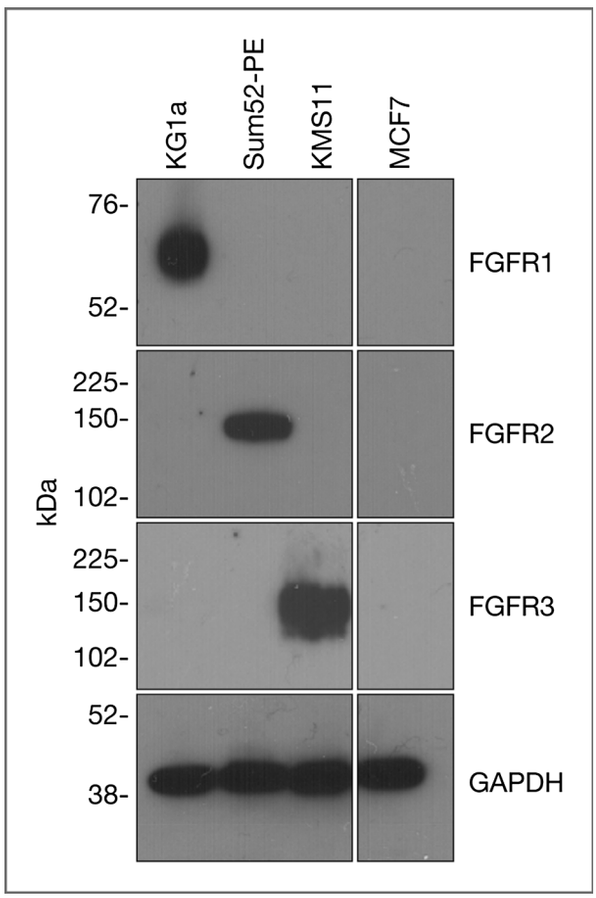

Figure 2. Inhibition of *in vitro* cell proliferation by AZD4547 correlates with deregulated FGFR expression in tumor cell lines. Western blot analyses confirming high expression of FGFR proteins from cell lines with known deregulations. GAPDH, glyceraldehyde-3-phosphate dehydrogenase.

AZD4547 has potent *in vitro* antiproliferative effects on tumor cell lines with deregulated FGFR expression

Three tumor cell lines were selected on the basis of known abnormalities in FGFR expression and signaling. KG1a is an acute myeloid leukemia cell line that expresses a truncated wild-type FGFR1 fusion protein (30); Sum52-PE is a breast cell line that expresses wild-type FGFR2 (31), and the KMS11 multiple myeloma line expresses a t(4;14) translocated/Y373C mutated FGFR3 protein (32). FGFR protein levels were assessed by Western blotting and overexpression was confirmed relative to a control cell line (MCF7) with no identified defects in FGFR expression or signaling (Fig. 2). The ability of AZD4547 to inhibit *in vitro* proliferation of these lines over a 3-day period was assessed with a standard metabolism-based proliferation assay. IC_{50} values ranged from 18 nmol/L in KG1a cells to 281 nmol/L in KMS11 cells (Table 2). Notably, MCF7 cell proliferation was unaffected by incubation with AZD4547 up to a concentration of 30 μmol/L. Moreover, AZD4547 was inactive against more than 100 additional tumor cell lines (Supplementary Table S1), showing that AZD4547 has potent *in vitro* antiproliferative activity only against tumor cell lines expressing deregulated FGFRs.

AZD4547 potently inhibits FGFR phosphorylation and downstream signaling in human tumor cell lines

To assess modulation of FGFR phosphorylation and signaling by AZD4547, cell lines were treated with drug and lysates analyzed by Western blotting. All 3 cell lines showed inhibition of FGFR and mitogen—activated protein kinase (MAPK) protein phosphorylation in a dose-dependent manner (Fig. 3A–C). With the exception of the KMS11 cell line, the concentrations of AZD4547 required to inhibit cellular FGFR phosphorylation were in good agreement with the *in vitro* proliferation IC_{50} values (Table 2). The phosphorylation of FRS2 and PLCγ, downstream markers of FGFR signaling, was also inhibited (Fig. 3D and E). Notably, AKT phosphorylation (which has been described to couple often to FGFR signaling) was unaffected by AZD4547 in KG1a and KMS11 lines but did show modulation by AZD4547 treatment in the breast cell lines, MCF7 (data not shown) and Sum52-PE. Thus, at the cellular level, AZD4547 potently inhibits FGFR phosphorylation and downstream signaling affected through FRS2, PLCγ, and MAPK.

The mechanism of growth inhibition by AZD4547 is cell line dependent

To understand the mechanism by which AZD4547 exerts antiproliferative activity *in vitro*, cellular Annexin V apoptosis assays, flow cytometric cell-cycle analysis, and Western blotting were conducted. Three drug concentrations were chosen (30 nmol/L, 100 nmol/L, and 1 μmol/L) to ensure good

Table 2. Summary of AZD4547 *in vitro* antiproliferative IC_{50} values obtained by MTS proliferation assay

Tumor cell line	Deregulated FGFR member	Proliferation IC_{50}, μmol/L	SEM
KG1a	FGFR1	0.018 ($n = 3$)	0.0017
Sum52-PE	FGFR2	0.041 ($n = 4$)	0.0185
KMS11	FGFR3	0.281 ($n = 5$)	0.0294
MCF7	None	>30 ($n = 6$)	NA

Abbreviation: NA, not applicable.

coverage of the approximate IC_{50} values for cellular proliferation and FGFR phosphorylation. Figure 4 shows the cell-cycle profiles of all 3 lines, following 3 days of treatment with AZD4547 (mean percent of cells in cell-cycle phase ± SEM, $n = 3$). KG1a cells show dramatic increase in the G_1 phase population upon treatment with all 3 doses of AZD4547 (Fig. 4A), with no increases in the sub-G_1 population. The Sum52-PE breast and KMS11 multiple myeloma cell lines both displayed an acute sensitivity to induction of cell death (sub-G_1 phase) following treatment with all doses of AZD4547 (Fig. 4B and C). Relative to untreated control cells, Annexin V staining confirmed significant apoptotic induction in Sum52-PE and KMS11 lines, but not in KG1a (Fig. 4D). Consistent with the lack of any *in vitro* antiproliferative effect of AZD4547 on the MCF7 breast cell line, no significant cell-cycle or apoptotic changes were observed following incubation with AZD4547 at any of the doses tested (Supplementary Fig. S1). Western blotting confirmed clear induction of the apoptotic markers, cleaved caspase-3, and PARP (Fig. 4E), in treated Sum52-PE and KMS11 lysates, but not in KG1a, consistent with the Annexin V and cell-cycle data. Further analysis showed increases in proapoptotic BIM protein levels in all 3 lines following AZD4547 treatment and high-level basal expression of the antiapoptotic protein Bcl2 in KG1a cells, but not in Sum52-PE or KMS11 (Fig. 4E).

Thus, at least in the lines tested here, cell fate in response to AZD4547 treatment is likely determined by the relative levels of key pro- and antiapoptotic proteins.

AZD4547 *in vivo* antitumor activity is associated with dose proportional pharmacodynamic modulation of phospho-FGFR3 and reduced KMS11 tumor cell proliferation

To assess AZD4547 *in vivo* efficacy, female SCID mice bearing KMS11 tumors were randomized and treated chronically with AZD4547 at a range of well-tolerated doses. Oral AZD4547 treatment resulted in dose-dependent tumor growth inhibition. Twice daily administration of AZD4547 at 3 mg/kg gave statistically significant tumor growth inhibition of 53% ($P < 0.0005$ by one-tailed t test) when compared with vehicle-treated controls, whereas doses of 12.5 mg/kg once daily and 6.25 mg/kg twice daily resulted in complete tumor stasis ($P < 0.0001$; Fig. 5A). A further efficacy study in the KG1a model with 12.5 mg/kg once daily AZD4547 resulted in 65% tumor growth inhibition ($P = 0.002$; Supplementary Fig. S2).

To assess *in vivo* modulation of FGFR phosphorylation, single doses of AZD4547 were orally administered to KMS11 tumor–bearing SCID mice and tumors harvested at various time points postdose for measurement of phosphorylated FGFR3 with a sandwich ELISA assay. Total plasma concentrations of AZD4547 clearly show a direct relationship with inhibition of FGFR3 phosphorylation within KMS11 tumors *in vivo* (Fig. 5B). A further study using a single 6.25 mg/kg dose of AZD4547 was conducted to define the duration and magnitude of the pharmacodynamic effect in tumors. Within 15 minutes of drug administration, the levels of phosphorylated FGFR3 decreased to 40% to 50% of control levels and inhibition was sustained for at least 6 hours. At the 16-hour time point, phosphorylated FGFR3 had returned to control levels (Fig. 5C). These data confirm good modulation of tumor phospho-FGFR3 levels for at least 6 hours, consistent with the plasma exposure of AZD4547.

To define the mechanism(s) through which AZD4547 elicits KMS11 tumor growth inhibition *in vivo*, KMS11 tumor–bearing mice were treated with 6.25 mg/kg AZD4547 twice daily for 7 days and tumors processed for immunohistochemical analysis. Tumor sections were stained using antibodies to cleaved caspase-3, Ki-67, and CD31, representing markers of cellular apoptosis, proliferation, and vascularity, respectively. AZD4547 treatment caused a significant reduction in the percentage of cells staining positive for nuclear Ki-67 (Fig. 5D and E). However, despite showing an increase in the AZD4547-treated sections, the difference in cleaved caspase-3 staining between controls versus AZD4547-treated tumor sections did not reach statistical significance. Similarly, AZD4547 treatment did not have any significant effect on CD31-positive vessel staining in KMS11 xenografts (Fig. 5D and E), showing that at efficacious dose levels, AZD4547 does not exhibit antiangiogenic effects. In summary, AZD4547 shows dose proportional antitumor efficacy in an FGFR3-driven xenograft model, concurrent with pharmacodynamic target modulation, and with evidence of a predominantly antiproliferative mechanism *in vivo*.

AZD4547 antitumor efficacy is not attributable to inhibition of KDR-driven functional effects *in vivo*

It is well documented that inhibition of VEGF signaling with agents such as cediranib (KDR inhibitor) can lead to hypertension (29, 33). Therefore, the effect of AZD4547 on blood pressure was measured in conscious telemetered rats. Two separate oral doses of 10 mg/kg AZD4547 over 24 hours did not lead to any significant changes in blood pressure compared

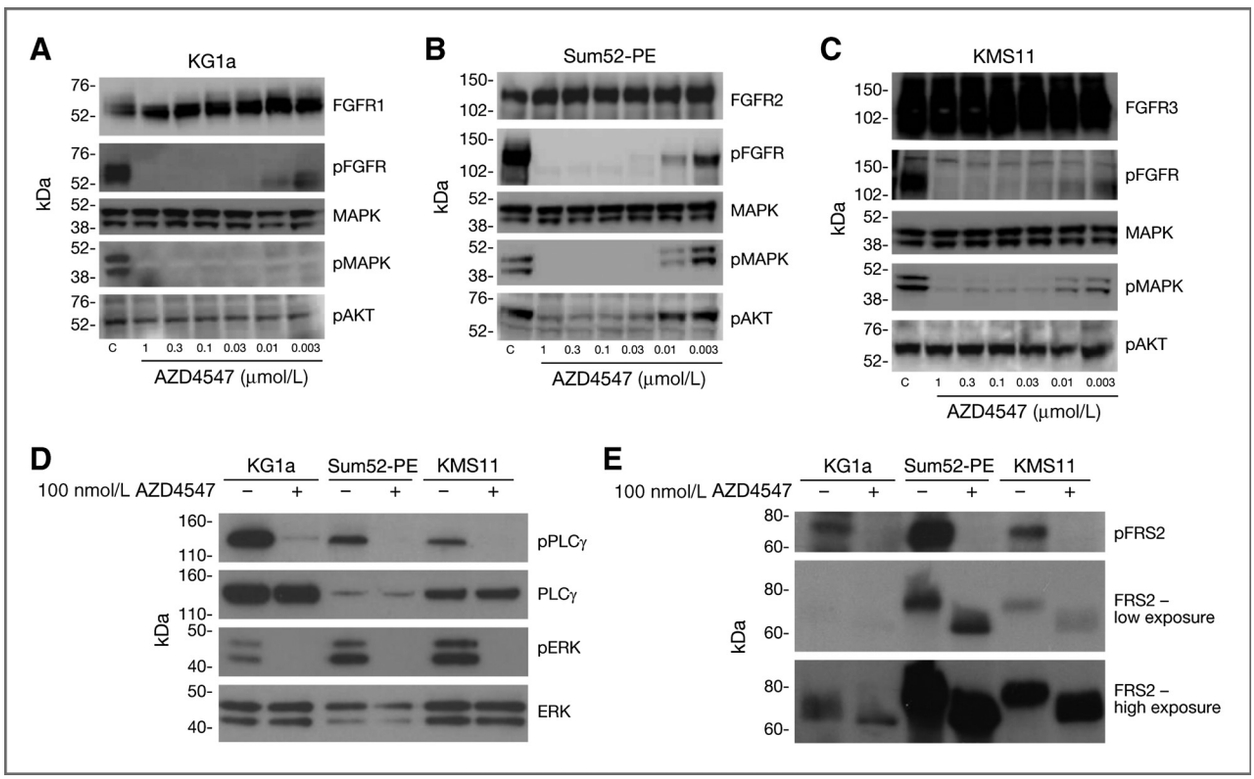

Figure 3. Inhibition of FGFR signaling by AZD4547. All cell lines were incubated for 3 hours with the stated AZD4547 concentrations and then stimulated with acidic FGF (aFGF)/basic FGF (bFGF; 10 ng/mL) and heparin (10 μg/mL) for 20 minutes. Cells were then lysed and immunoblotted for the proteins indicated. A–C, KMS11, Sum52-PE, and KG1a were analyzed for total FGFR1–3, phospho- and total FGFR, MAPK, and AKT. D, phospho- and total PLCγ, and Erk. E, phospho- and total FRS2.

with vehicle-dosed animals (Fig. 6A represents the diastolic pressure for vehicle control and AZD4547). The free plasma exposure of AZD4547 after dosing at 10 mg/kg in rats is equivalent to the exposure in mouse, which results in greater than 60% tumor growth inhibition in the KMS11 model. These data show that at equivalent efficacious doses, AZD4547 has no significant effect on blood pressure and therefore lacks *in vivo* anti-KDR activity.

Broad antitumor efficacy in preclinical xenograft models is a feature of agents, which act predominantly through antiangiogenic mechanisms. To examine the breadth of its activity, AZD4547 was assessed in a number of models that have been shown to be sensitive to inhibitors of VEGF signaling, such as cediranib (28). Mice bearing Calu-6 (lung) tumors were treated chronically with either 3 mg/kg cediranib once daily or 6.25 mg/kg AZD4547 twice daily. Cediranib resulted in significant tumor growth inhibition (64%), which is consistent with previous reports (28); however, AZD4547 lacked efficacy in this model (Fig. 6B). Similarly, dosing of 6.25 mg/kg orally twice daily AZD4547 was also inactive in 2 additional cediranib-sensitive xenograft models—HCT-15 and LoVo (Table 3).

Taken together, the telemetry, immunohistochemical, and efficacy data suggest that the antitumor effects of AZD4547 are not likely to be attributable to inhibition of KDR activity and are a result of its potent and selective FGFR profile.

Discussion

This report provides the first pharmacologic profile of the pyrazoloamide derivative, AZD4547, an orally bioavailable selective inhibitor of FGFR tyrosine kinases with potential as a targeted antitumor therapy.

AZD4547 is a potent inhibitor of FGFR tyrosine kinases 1, 2, and 3 and is also selective versus a range of other related kinases, such as KDR, IGF, PI3Ka, and AKT. Potent nanomolar IC_{50} values were obtained when AZD4547 was examined against recombinant FGFR kinases (FGFR1, IC_{50} = 0.2 nmol/L), whereas activity versus KDR was approximately 120-fold lower (KDR, IC_{50} = 24 nmol/L). Cellular phosphorylation data confirmed this dominant FGFR selectivity profile with an approximate 20-fold difference over KDR (FGFR1, cellular IC_{50} = 12 nmol/L; KDR, cellular IC_{50} = 258 nmol/L).

Our data show that AZD4547 is a potent cell growth inhibitor versus tumor cell lines with known irregularities in FGFR expression. Several studies have indirectly established that elevated FGFR protein levels correlate with receptor ligand independence and result in mitogenic growth (10–13). Qian and colleagues have previously validated FGFR3 as a proliferative driver within the KMS11 multiple myeloma cell line, which contains mutated (Y373C) and overexpressed FGFR3

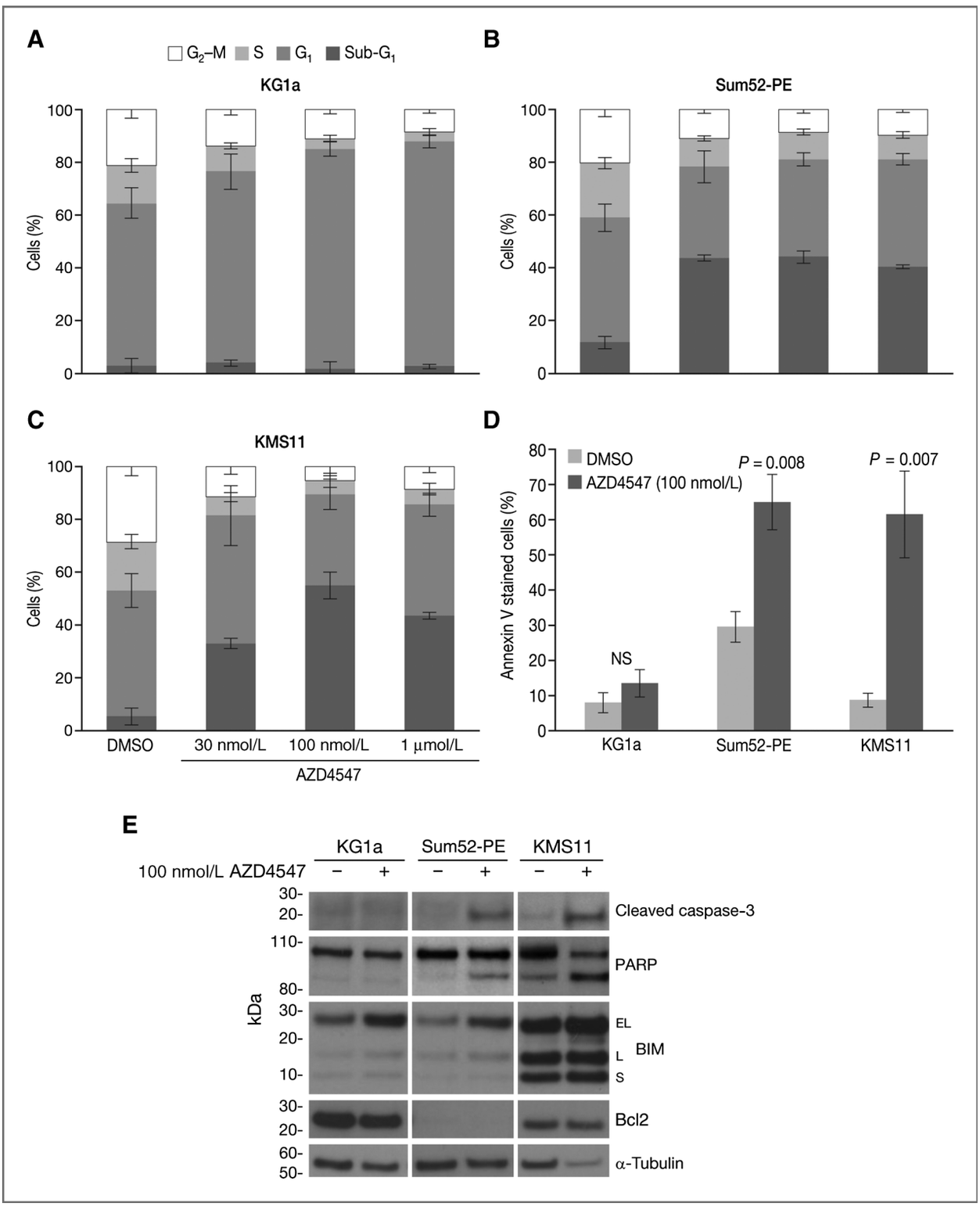

Figure 4. The mechanism of *in vitro* growth inhibition by AZD4547 is cell line–dependent. A–C, cells were exposed to AZD4547 for 72 hours and then analyzed for their cell-cycle distribution using propidium iodide and a FACSCalibur flow cytometric system. D, quantified Annexin V flow cytometric data from cells treated *in vitro* with 100 nmol/L AZD4547 for 72 hours. *P* values were calculated using the Student *t* test and refer to the comparison between dimethyl sulfoxide (DMSO) and AZD4547 for each cell line. Data are representative of 3 independent experiments. NS, not significant. E, cells were exposed to 100 nmol/L AZD4547 for 72 hours and then lysed and immunoblotted for the proteins indicated.

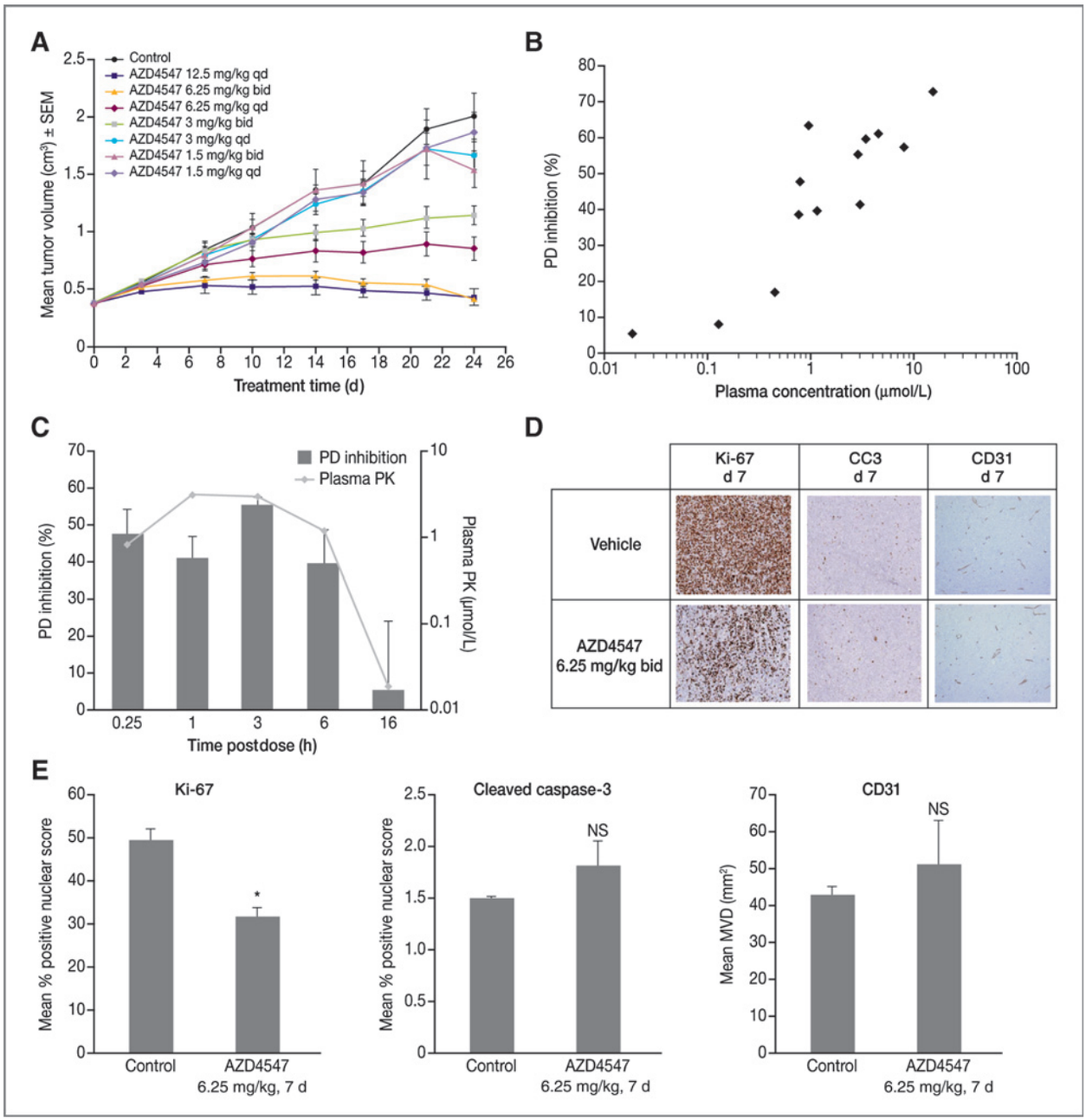

Figure 5. AZD4547 exposure correlates with *in vivo* antitumor activity, pharmacodynamic modulation of phospho-FGFR, and reduced tumor cell proliferation. A, AZD4547 was administered by oral gavage once (qd) or twice (bid) daily to SCID mice bearing established s.c. KMS11 human tumor xenografts at the doses indicated. Tumor volumes are plotted against time. B, pharmacokinetic (PK)/pharmacodynamic relationship in KMS11 xenograft. AZD4547 was dosed orally at a range of concentrations, and tumors and blood collected at various time points for ELISA analysis of phospho-FGFR3 and AZD4547 drug levels, respectively. Total plasma drug levels and the percentage inhibition of phospho-FGFR3 (PD inhibition) compared with control are plotted. C, AZD4547 was dosed orally at 6.25 mg/kg (single dose) and plasma and tumors collected over a 16-hour time course. D, Ki-67, cleaved caspase-3 (CC3), and CD31 immunohistochemical staining of KMS11 tumor sections removed after 7 days twice daily dosing of 6.25 mg/kg AZD4547 (4 hours after final dose). E, image analysis data for Ki-67, CC3, and CD31 immunostained tumors showing mean values for each group ($n = 4$ animals per group). Ki-67 shows statistical significance with one-tailed t test. *, $P = 0.012$. NS, not significant.

(34, 35). This mutation activates FGFR3 through ligand-independent constitutive dimerization. Similarly, both KG1a and Sum52-PE cell lines exhibit a dependence on FGFR1 and 2 signaling respectively for proliferation, as shown by siRNA (30) and the selective commercially available FGFR inhibitor, PD173074 (10). In cell culture, we were able to confirm deregulation of FGFR protein expression within several "oncogene addicted" human tumor cell lines and show their exquisite

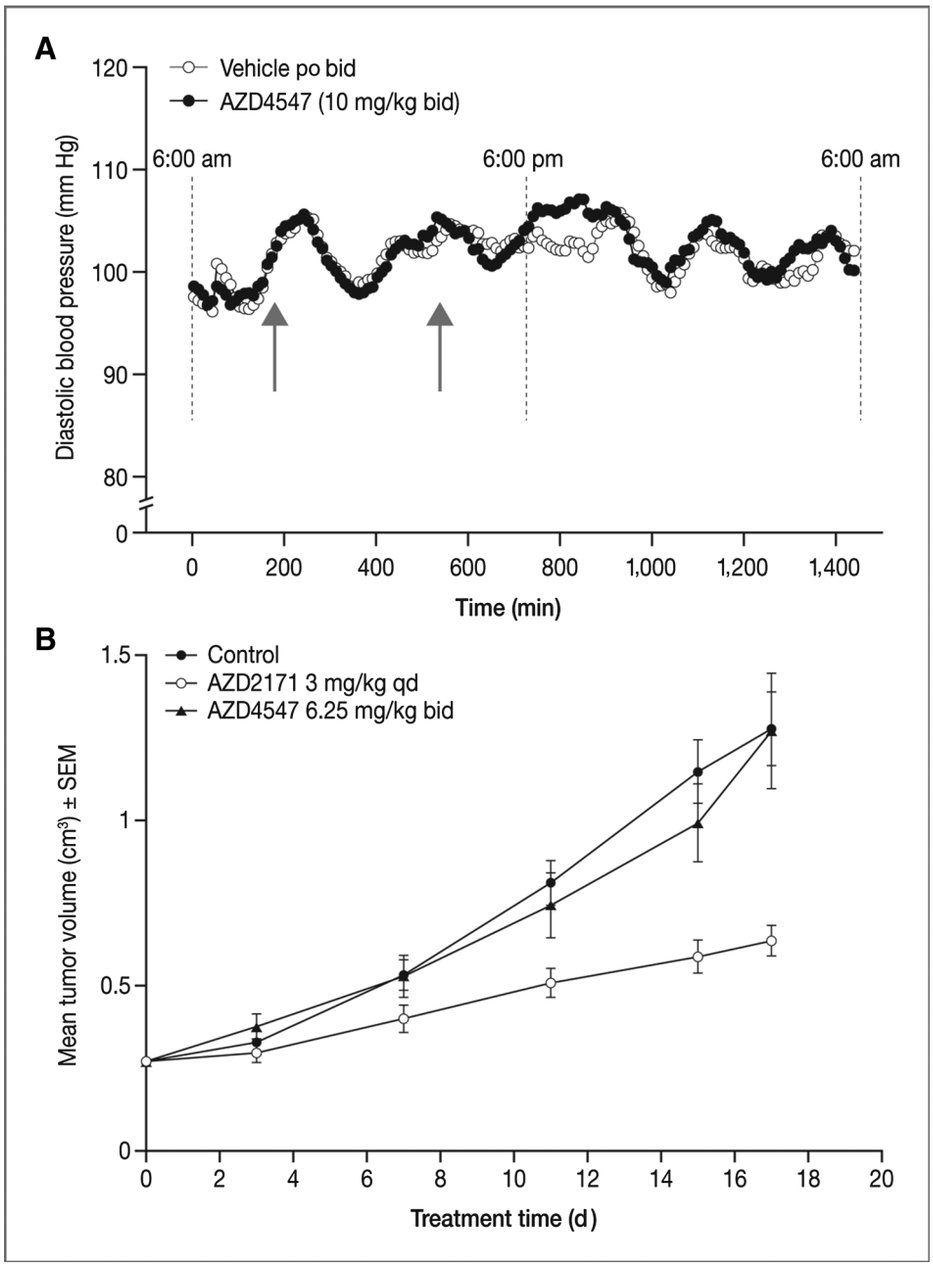

Figure 6. AZD4547 antitumor efficacy is not attributable to inhibition of KDR. A, mean diastolic blood pressure measurements of a group of unrestrained conscious telemetered rats ($n = 3$) given 2 oral doses at 180 and 540 minutes (arrows): on day 1, vehicle control (o) and the following day (day 2) AZD4547 at 10 mg/kg (●). bid, twice daily; po, orally. B, nude mice bearing established Calu-6 human tumor xenografts were treated orally, twice daily with AZD4547 (6.25 mg/kg) or cediranib (3 mg/kg) once daily.

antiproliferative sensitivity to AZD4547. Our chosen cell lines represent both wild-type and point-mutated FGFR proteins, indicating that AZD4547 is active against the tyrosine kinase activity of both the wild-type and mutant forms of FGFR used here. Importantly, the lack of any AZD4547 antiproliferative effects in FGFR nonderegulated tumor cell lines (including MCF7) indicates a lack of nonspecific cytotoxicity within the effective drug concentration range.

AZD4547 inhibits FGFR downstream signaling and induces both cytostatic and cytotoxic effects dependent upon the cellular background. In the cell lines tested here, incubation with AZD4547 resulted in potent inhibition of cellular FGFR1, FGFR2, FGFR3, FRS2, and PLCγ phosphorylation, whereas concomitant inhibition of pMAPK confirmed that FGFR signaling remains coupled to the MAPK cascade [AZD4547 is inactive vs. recombinant MAP–extracellular signal—regulated (ERK) kinase (MEK) and MAPK enzymes; data not shown]. This requirement for a coupled FGFR-MAPK signaling pathway suggests clear implications for an AZD4547 clinical patient selection strategy. Activating mutations within the *ras* gene family occur with a frequency of up to 30% across a diverse range of human tumors (36, 37) and, in the case of FGFR, circumvent the dependence of cells on ligand-induced stimulation (11). However, the mutual exclusivity of FGFR and Ras mutations observed across several tumor types, including pancreatic (38), multiple myeloma (39), and urothelial

Table 3. Tumor growth inhibition in nude mice bearing established Calu-6 human tumor xenografts

	Inhibition of tumor growth, %	
Tumor model	**AZD4547**	**Cediranib[a]**
LoVo	0	63
HCT-15	4.7	82[b]

NOTE: Mice were treated orally, twice daily with AZD4547 (6.25 mg/kg) for 14 to 17 days or cediranib (LoVo, 1.5 mg/kg; Calu-6, 6 mg/kg; HCT-15, 6 mg/kg) once daily for up to 28 days. Percentage of tumor growth inhibition was calculated as the difference between the mean change in control versus treated tumor volumes over the period of treatment.
[a]Data previously published.
[b]Unpublished data.

carcinoma (40), suggests that these oncogenes use common signaling pathways to maintain the tumor phenotype. Because tumor growth driven by deregulated FGFR expression (and hence sensitive to AZD4547) is unlikely to be reliant on mutant Ras signaling, a patient selection strategy based on deregulated FGFR alone is suggested.

Sum52-PE breast cancer cells are dependent on FGFR2 signaling to activate signal transduction pathways involving FRS2, MAPK, and phosphoinositide 3-kinase (PI3K; ref. 10). Published data support a key role for FRS2 signaling in activating both the MAPK to induce cell proliferation and differentiation and also PI3K to activate cell survival pathways (41). Consistent with these data, AZD4547 shows potent inhibition of both pERK and pAKT cellular phosphorylation and concomitant induction of apoptosis in Sum52-PE cells. The lack of pAKT modulation by AZD4547 in KG1a and KMS11 cells, however, is likely explained by the finding that PI3K and AKT are overactivated in most myeloma and leukemia cell lines (42). Indeed, KG1a cells are known to contain a hypermethylated *PTEN* promoter (43), whereas KMS11 harbors a constitutively active AKT (42). As neither line shows modulation of pAKT by AZD4547, we suggest that the antiproliferative versus apoptotic response to AZD4547 is modulated by the relative balance of pro- and antiapoptotic proteins. In KG1a cells, although AZD4547 treatment induces an increase in proapoptotic BIM expression, the relatively high level of antiapoptotic Bcl2 protein would appear to protect against apoptotic induction. Conversely, within Sum52-PE and KMS11 cells, despite induction of BIM expression by AZD4547, basal Bcl2 levels remain low or undetectable, thus allowing apoptosis to occur in these lines. Accordingly, at least in the lines tested here, we propose that AZD4547 induces apoptosis via induction of BIM expression only in those lines where levels of the antiapoptotic protein Bcl2 are low or undetectable.

In preclinical xenograft models, AZD4547 exposure correlated with *in vivo* antitumor efficacy and pharmacodynamic modulation of target and proliferation endpoints. Dose-related AZD4547 efficacy was shown in SCID mice bearing established KMS11 tumors (99% tumor growth inhibition with 6.25 mg/kg twice daily dosing). Despite observing substantial *in vivo* inhibition of phospho-FGFR3 levels in KMS11 tumors at a dose of 6.25 mg/kg, we were unable to confirm statistically significant apoptotic induction by a cleaved caspase-3 immunohistochemical endpoint but did observe a significant reduction in Ki-67 tumor staining. The apparent phenotypic disconnect observed here between potent induction of KMS11 cell apoptosis by AZD4547 *in vitro*, compared with slowed growth in the absence of any detectable apoptosis *in vivo*, may be explained by the time points of tumor sampling. Immunohistochemical staining for Ki-67 and CC3 was conducted on tumors after 7 days of AZD4547 treatment, which, based on the AZD4547 antitumor preclinical efficacy data, describes a phase of slowed tumor growth but precedes any tumor stasis effects (observed at >14 days). Indeed, this interpretation is supported by similar studies using PD173074 where low *in vitro* concentrations resulted in KMS11 cell apoptosis after 4 days of incubation, while *in vivo* apoptotic markers only became visible within KMS11 xenograft sections after 9 days of twice daily dosing (44). Further work is currently underway to confirm this interpretation and investigate the time dependency of the pharmacodynamic changes elicited by AZD4547.

The *in vivo* data presented here are consistent with AZD4547 being a predominantly FGFR-selective small-molecule inhibitor. Treatment with AZD4547 did not result in the well-characterized blood pressure changes associated with acute KDR inhibition in telemetered rat studies (29, 33). Furthermore, we detected no significant changes in CD31 immunohistochemical staining in KMS11 tumor xenograft sections at an efficacious dose and time point, nor were we able to show efficacy in KDR-sensitive xenograft tumor models. Accordingly, we believe that AZD4547 is capable of clinically testing an FGFR tumor–driven hypothesis, aiming to select patients based on deregulated tumor FGFR expression.

In summary, using a panel of tumor cell lines *in vitro*, we have shown that endogenous FGFR protein expression levels predict antiproliferative sensitivity to the novel, potent FGFR-selective agent, AZD4547. Our data show potent modulation of phospho-FGFR signaling within FGFR-deregulated cell lines and highlight both proapoptotic and antiproliferative phenotypes, dictated by the relative expressions of key pro- and antiapoptotic proteins. AZD4547 inhibits the growth of KMS11 tumor xenografts at doses (and plasma exposure), which cause pharmacodynamic modulation of tumor phospho-FGFR. Furthermore, AZD4547 shows no *in vivo* evidence of anti-KDR–related efficacy or physiology and is well-tolerated. These data support further investigation of AZD4547 as a targeted therapeutic option for patients with tumors harboring deregulated FGFR expression. AZD4547 is currently being evaluated in phase I clinical trials.

Disclosure of Potential Conflicts of Interest

P.R. Gavine and T. Klinowska have employment (other than primary affiliation; e.g., consulting) with AstraZeneca as the principal scientists. A.N. Brooks

has ownership interest (including patents) from AstraZeneca. No potential conflicts of interests were disclosed by the other authors.

Authors' Contributions

Conception and design: P.R. Gavine, L. Mooney, A.P. Thomas, A.N. Brooks, T. Klinowska
Development of methodology: P.R. Gavine, C. Rooney, T. Klinowska
Acquisition of data: P.R. Gavine, L. Mooney, K. Al-Kadhimi, S. Beck, C. Rooney, T. Coleman, T. Klinowska
Analysis and interpretation of data: P.R. Gavine, L. Mooney, C. Rooney, T. Coleman, D. Baker, M.J. Mellor, A.N. Brooks, T. Klinowska
Writing, review, and/or revision of the manuscript: P.R. Gavine, L. Mooney, E. Kilgour, A.P. Thomas, K. Al-Kadhimi, T. Coleman, M.J. Mellor, A.N. Brooks, T. Klinowska
Administrative, technical, or material support: P.R. Gavine, D. Baker
Study supervision: E. Kilgour, A.N. Brooks, T. Klinowska

Acknowledgments

The authors thank Nahida Parveen, Jon Orme, Jon Curwen, Helen Musgrove, Jeremy Frith, Keith Welsh, Neil Smith, Mike Dennis, David Buttar, Gail Wrigley (née Young), Linette Ruston, Maria-Elena Theoclitou, and Ray Gairns for their technical assistance and involvement in this study. Figure design support was provided by Mudskipper Bioscience, funded by AstraZeneca.

Grant Support

This research was conducted and funded by AstraZeneca.

The costs of publication of this article were defrayed in part by the payment of page charges. This article must therefore be hereby marked *advertisement* in accordance with 18 U.S.C. Section 1734 solely to indicate this fact.

Received September 9, 2011; revised January 14, 2012; accepted February 2, 2012; published OnlineFirst February 27, 2012.

References

1. Klint P, Claesson-Welsh L. Signal transduction by fibroblast growth factor receptors. Front Biosci 1999;4:D165–77.
2. Plotnikov AN, Hubbard SR, Schlessinger J, Mohammadi M. Crystal structures of two FGF-FGFR complexes reveal the determinants of ligand-receptor specificity. Cell 2000;101:413–24.
3. Ray ME, Yang ZQ, Albertson D, Kleer CG, Washburn JG, Macoska JA, et al. Genomic and expression analysis of the 8p11-12 amplicon in human breast cancer cell lines. Cancer Res 2004;64:40–7.
4. Keats JJ, Reiman T, Belch AR, Pilarski LM. Ten years and counting: so what do we know about t(4;14)(p16;q32) multiple myeloma. Leuk Lymphoma 2006;47:2289–300.
5. Billerey C, Chopin D, ubriot-Lorton MH, Ricol D, Gil Diez de Medina S, Van RB, et al. Frequent FGFR3 mutations in papillary non-invasive bladder (pTa) tumors. Am J Pathol 2001;158:1955–9.
6. Pollock PM, Gartside MG, Dejeza LC, Powell MA, Mallon MA, Davies H, et al. Frequent activating FGFR2 mutations in endometrial carcinomas parallel germline mutations associated with craniosynostosis and skeletal dysplasia syndromes. Oncogene 2007;26:7158–62.
7. Jang JH, Shin KH, Park JG. Mutations in fibroblast growth factor receptor 2 and fibroblast growth factor receptor 3 genes associated with human gastric and colorectal cancers. Cancer Res 2001;61:3541–3.
8. Sahadevan K, Darby S, Leung HY, Mathers ME, Robson CN, Gnanapragasam VJ. Selective overexpression of fibroblast growth factor receptors 1 and 4 in clinical prostate cancer. J Pathol 2007;213:82–90.
9. Plowright EE, Li Z, Bergsagel PL, Chesi M, Barber DL, Branch DR, et al. Ectopic expression of fibroblast growth factor receptor 3 promotes myeloma cell proliferation and prevents apoptosis. Blood 2000;95:992–8.
10. Moffa AB, Tannheimer SL, Ethier SP. Transforming potential of alternatively spliced variants of fibroblast growth factor receptor 2 in human mammary epithelial cells. Mol Cancer Res 2004;2:643–52.
11. Trudel S, Li ZH, Wei E, Wiesmann M, Chang H, Chen C, et al. CHIR-258, a novel, multitargeted tyrosine kinase inhibitor for the potential treatment of t(4;14) multiple myeloma. Blood 2005;105:2941–8.
12. Naski MC, Wang Q, Xu J, Ornitz DM. Graded activation of fibroblast growth factor receptor 3 by mutations causing achondroplasia and thanatophoric dysplasia. Nat Genet 1996;13:233–7.
13. Kunii K, Davis L, Gorenstein J, Hatch H, Yashiro M, Di Bacco A, et al. FGFR2-amplified gastric cancer cell lines require FGFR2 and Erbb3 signaling for growth and survival. Cancer Res 2008;68:2340–8.
14. Li Y, Mangasarian K, Mansukhani A, Basilico C. Activation of FGF receptors by mutations in the transmembrane domain. Oncogene 1997;14:1397–406.
15. Popovici C, Zhang B, Gregoire MJ, Jonveaux P, Lafage-Pochitaloff M, Birnbaum D, et al. The t(6;8)(q27;p11) translocation in a stem cell myeloproliferative disorder fuses a novel gene, FOP, to fibroblast growth factor receptor 1. Blood 1999;93:1381–9.
16. Reiter A, Sohal J, Kulkarni S, Chase A, Macdonald DH, Aguiar RC, et al. Consistent fusion of ZNF198 to the fibroblast growth factor receptor-1 in the t(8;13)(p11;q12) myeloproliferative syndrome. Blood 1998;92:1735–42.
17. Demiroglu A, Steer EJ, Heath C, Taylor K, Bentley M, Allen SL, et al. The t(8;22) in chronic myeloid leukemia fuses BCR to FGFR1: transforming activity and specific inhibition of FGFR1 fusion proteins. Blood 2001;98:3778–83.
18. Song S, Wientjes MG, Gan Y, Au JL. Fibroblast growth factors: an epigenetic mechanism of broad spectrum resistance to anticancer drugs. Proc Natl Acad Sci U S A 2000;97:8658–63.
19. Pardo OE, Wellbrock C, Khanzada UK, Aubert M, Arozarena I, Davidson S, et al. FGF-2 protects small cell lung cancer cells from apoptosis through a complex involving PKCepsilon, B-Raf and S6K2. EMBO J 2006;25:3078–88.
20. Pardo OE, Arcaro A, Salerno G, Raguz S, Downward J, Seckl MJ. Fibroblast growth factor-2 induces translational regulation of Bcl-XL and Bcl-2 via a MEK-dependent pathway: correlation with resistance to etoposide-induced apoptosis. J Biol Chem 2002;277:12040–6.
21. Roidl A, Berger HJ, Kumar S, Bange J, Knyazev P, Ullrich A. Resistance to chemotherapy is associated with fibroblast growth factor receptor 4 up-regulation. Clin Cancer Res 2009;15:2058–66.
22. Batchelor TT, Sorensen AG, di Tomaso E, Zhang WT, Duda DG, Cohen KS, et al. AZD2171, a pan-VEGF receptor tyrosine kinase inhibitor, normalizes tumor vasculature and alleviates edema in glioblastoma patients. Cancer Cell 2007;11:83–95.
23. Yoshiji H, Harris SR, Thorgeirsson UP. Vascular endothelial growth factor is essential for initial but not continued *in vivo* growth of human breast carcinoma cells. Cancer Res 1997;57:3924–8.
24. Huynh H, Ngo VC, Fargnoli J, Ayers M, Soo KC, Koong HN, et al. Brivanib alaninate, a dual inhibitor of vascular endothelial growth factor receptor and fibroblast growth factor receptor tyrosine kinases, induces growth inhibition in mouse models of human hepatocellular carcinoma. Clin Cancer Res 2008;14:6146–53.
25. Hilberg F, Roth GJ, Krssak M, Kautschitsch S, Sommergruber W, Tontsch-Grunt U, et al. BIBF 1120: triple angiokinase inhibitor with sustained receptor blockade and good antitumor efficacy. Cancer Res 2008;68:4774–82.
26. Fabbro D, Manley PW. Su-6668. SUGEN. Curr Opin Investig Drugs 2001;2:1142–8.
27. Davies BR, Logie A, McKay JS, Martin P, Steele S, Jenkins R, et al. AZD6244 (ARRY-142886), a potent inhibitor of mitogen-activated protein kinase/extracellular signal-regulated kinase kinase 1/2 kinases: mechanism of action *in vivo*, pharmacokinetic/pharmacodynamic relationship, and potential for combination in preclinical models. Mol Cancer Ther 2007;6:2209–19.
28. Wedge SR, Kendrew J, Hennequin LF, Valentine PJ, Barry ST, Brave SR, et al. AZD2171: a highly potent, orally bioavailable, vascular endothelial growth factor receptor-2 tyrosine kinase inhibitor for the treatment of cancer. Cancer Res 2005;65:4389–400.

29. Curwen JO, Musgrove HL, Kendrew J, Richmond GH, Ogilvie DJ, Wedge SR. Inhibition of vascular endothelial growth factor-A signaling induces hypertension: examining the effect of cediranib (Recentin; AZD2171) treatment on blood pressure in rat and the use of concomitant antihypertensive therapy. Clin Cancer Res 2008;14:3124–31.
30. Gu TL, Goss VL, Reeves C, Popova L, Nardone J, Macneill J, et al. Phosphotyrosine profiling identifies the KG-1 cell line as a model for the study of FGFR1 fusions in acute myeloid leukemia. Blood 2006;108:4202–4.
31. Tannheimer SL, Rehemtulla A, Ethier SP. Characterization of fibroblast growth factor receptor 2 overexpression in the human breast cancer cell line SUM-52PE. Breast Cancer Res 2000;2:311–20.
32. Chesi M, Brents LA, Ely SA, Bais C, Robbiani DF, Mesri EA, et al. Activated fibroblast growth factor receptor 3 is an oncogene that contributes to tumor progression in multiple myeloma. Blood 2001; 97:729–36.
33. Maitland ML, Kasza KE, Karrison T, Moshier K, Sit L, Black HR, et al. Ambulatory monitoring detects sorafenib-induced blood pressure elevations on the first day of treatment. Clin Cancer Res 2009;15:6250–7.
34. Qian S, Somlo G, Zhou B, Zhu L, Mi S, Mo X, et al. Ribozyme cleavage leads to decreased expression of fibroblast growth factor receptor 3 in human multiple myeloma cells, which is associated with apoptosis and downregulation of vascular endothelial growth factor. Oligonucleotides 2005;15:1–11.
35. Zhu L, Somlo G, Zhou B, Shao J, Bedell V, Slovak ML, et al. Fibroblast growth factor receptor 3 inhibition by short hairpin RNAs leads to apoptosis in multiple myeloma. Mol Cancer Ther 2005;4:787–98.
36. Adjei AA. Blocking oncogenic Ras signaling for cancer therapy. J Natl Cancer Inst 2001;93:1062–74.
37. Karnoub AE, Weinberg RA. Ras oncogenes: split personalities. Nat Rev Mol Cell Biol 2008;9:517–31.
38. Byron SA, Gartside MG, Wellens CL, Mallon MA, Keenan JB, Powell MA, et al. Inhibition of activated fibroblast growth factor receptor 2 in endometrial cancer cells induces cell death despite PTEN abrogation. Cancer Res 2008;68:6902–7.
39. Chesi M, Nardini E, Brents LA, Schrock E, Ried T, Kuehl WM, et al. Frequent translocation t(4;14)(p16.3;q32.3) in multiple myeloma is associated with increased expression and activating mutations of fibroblast growth factor receptor 3. Nat Genet 1997;16:260–4.
40. Jebar AH, Hurst CD, Tomlinson DC, Johnston C, Taylor CF, Knowles MA. FGFR3 and Ras gene mutations are mutually exclusive genetic events in urothelial cell carcinoma. Oncogene 2005;24:5218–25.
41. Ong SH, Hadari YR, Gotoh N, Guy GR, Schlessinger J, Lax I. Stimulation of phosphatidylinositol 3-kinase by fibroblast growth factor receptors is mediated by coordinated recruitment of multiple docking proteins. Proc Natl Acad Sci U S A 2001;98:6074–9.
42. Mao X, Cao B, Wood TE, Hurren R, Tong J, Wang X, et al. A small-molecule inhibitor of D-cyclin transactivation displays preclinical efficacy in myeloma and leukemia via phosphoinositide 3-kinase pathway. Blood 2011;117:1986–97.
43. Li M, Liu H, Xu ZF, Liu XR, Wang Y, Rao Q, et al. [Promoter methylation status of PTEN gene and the effect of induced demethylation in leukemia cell lines]. Zhonghua Xue Ye Xue Za Zhi 2008; 29:289–92.
44. Trudel S, Ely S, Farooqi Y, Affer M, Robbiani DF, Chesi M, et al. Inhibition of fibroblast growth factor receptor 3 induces differentiation and apoptosis in t(4;14) myeloma. Blood 2004;103:3521–8.